

A 10 year climatology of Arctic cloud fraction and radiative forcing at Barrow, Alaska

Xiquan Dong,¹ Baike Xi,¹ Kathryn Crosby,¹ Charles N. Long,² Robert S. Stone,^{3,4} and Matthew D. Shupe^{3,4}

Received 3 November 2009; revised 2 April 2010; accepted 13 April 2010; published 15 September 2010.

[1] A 10 year record of Arctic cloud fraction and radiative forcing has been generated using data collected at the Atmospheric Radiation Measurement (ARM) North Slope of Alaska site and the nearby NOAA Barrow Observatory (BRW) from June 1998 to May 2008. The cloud fractions (CFs) derived from ARM radar-lidar and ceilometer measurements increase significantly from March to May (0.57→0.84), remain relatively high (~0.80–0.9) from May to October, and then decrease from November to the following March (0.8→0.57), having an annual average of 0.76. These CFs are comparable to those derived from ground-based radar-lidar observations during the Surface Heat Budget of the Arctic Ocean experiment and from satellite observations over the western Arctic regions. The monthly means of estimated clear-sky and measured all-sky shortwave (SW)-down and longwave (LW)-down fluxes at the two facilities are almost identical with the annual mean differences less than 1.6 Wm^{-2} . Values of LW cloud radiative forcing (CRF) are minimum (6 Wm^{-2}) in March, then increase monotonically to reach maximum (63 Wm^{-2}) in August, then decrease continuously to the following March. The cycle of SW CRF mirrors its LW counterpart with the greatest negative impact occurring during the snow-free months of July and August. On annual average, the negative SW CRFs and positive LW CRFs nearly cancel, resulting in annual average NET CRF of about 3.5 Wm^{-2} on the basis of the combined ARM and BRW analysis. Compared with other studies, we find that LW CRF does not change over the Arctic regions significantly, but NET CRFs change from negative to positive from Alaska to the Beaufort Sea, indicating that Barrow is at a critical latitude for neutral NET CRF. The sensitivity study has shown that LW CRFs increase with increasing cloud fraction, liquid water path, and radiating temperature with high positive correlations (0.8–0.9). Negative correlations are found for SW CRFs, but a strong positive correlation between SW CRF and surface albedo exists.

Citation: Dong, X., B. Xi, K. Crosby, C. N. Long, R. S. Stone, and M. D. Shupe (2010), A 10 year climatology of Arctic cloud fraction and radiative forcing at Barrow, Alaska, *J. Geophys. Res.*, 115, D17212, doi:10.1029/2009JD013489.

1. Introduction

[2] The Arctic plays a major role in global climate through interactions between its atmosphere, snow/ice-covered land surfaces and ocean and coupled feedbacks [Randall *et al.*, 1998; Curry *et al.*, 1996, 2000; Stamnes *et al.*, 1999]. The cloud-radiative interactions in the Arctic are very complex due to low temperatures and absolute humidity, large solar

zenith angles, the presence of the highly reflective and inhomogeneous snow/ice surfaces and multilayered clouds, and persistent temperature inversions [Curry *et al.*, 1996]. The importance of cloud-radiation interactions to global climate has been highlighted by many investigators [e.g., Wetherald and Manabe, 1988; Mitchell and Ingram, 1992], and recent climate modeling results have revealed that the largest disagreement between coupled climate model simulations of present-day climate is found in the Arctic region [Gates, 1992; Tao *et al.*, 1996].

[3] Clouds and radiation are recognized as important issues with regard to Arctic climate and significant work has been accomplished in this area, such as the First International Satellite Cloud Climatology Project Regional Experiment Arctic Cloud Experiment [Curry *et al.*, 2000], the Surface Heat Budget of the Arctic Ocean project (SHEBA) [Perovich *et al.*, 1999; Uttal *et al.*, 2002], and the Mixed-Phase Arctic Cloud Experiment [Verlinde *et al.*, 2007]. However, there

¹Department of Atmospheric Sciences, University of North Dakota, Grand Forks, North Dakota, USA.

²Pacific Northwest National Laboratory, U.S. Department of Energy, Richland, Washington, USA.

³Cooperative Institute for Research in Environmental Sciences, University of Colorado at Boulder, Boulder, Colorado, USA.

⁴National Oceanic and Atmospheric Administration Earth System Research Laboratory, Boulder, Colorado, USA.

still exist large gaps in our understanding of how the physical and dynamical processes of Arctic clouds impact the surface radiation budget (SRB). Characterizing cloud effects on the surface radiation budget is critical for understanding the current climate and an important step toward simulating potential climate change. It is especially important over the Arctic region because it can significantly affect the melting, refreezing, thickness, and distribution of the seasonal ice pack [Maykut and Untersteiner, 1971]. Therefore, it is necessary to have statistically reliable results describing Arctic clouds and the surface radiation budget based on long-term surface observations.

[4] There are growing concerns about the decline in Arctic sea ice manifested by extremes in summer retreat and a thinning ice pack overall. These trends are indicators of climate change according to many recent studies. For example, Stroeve *et al.* [2008] estimated that the Arctic ice extent in September 2007 decreased by 50% compared with conditions from the 1950s to the 1970s, or was 37% lower than the 1979–2006 average [Comiso *et al.*, 2008], establishing a new record minimum. During summer 2007, an anomalous high pressure located over the Beaufort Sea resulted in relatively clear skies and more shortwave (SW)-down flux. Kay *et al.* [2008] illustrated that reduced cloud fractions and enhanced SW-down flux contributed significantly to the 2007 record minimum sea ice extent. Schweiger *et al.* [2008], however, used an ice-ocean model to demonstrate that reduced cloud fractions and enhanced SW-down flux contributed little to the 2007 record minimum sea ice extent, claiming that the impact of enhanced SW was small and largely confined to areas north of the ice edge, where albedos were high and thus additional solar absorption was minimal.

[5] To provide more observational evidence related to these investigations of Arctic clouds and SRB, we document the seasonal variation of cloud fraction, radiative flux, and cloud radiative forcing (CRF) using data collected from June 1998 to May 2008 at the Department of Energy Atmospheric Radiation Measurement (ARM) Program [Ackerman and Stokes, 2003; Stamnes *et al.*, 1999] North Slope of Alaska (NSA) site and the National Oceanic and Atmospheric Administration (NOAA) Earth System Research Laboratory (ESRL) Barrow Observatory (BRW). The present work, which uses the first nearly continuous set of 10 year ground-based radiation and comprehensive cloud observations, should provide the most reliable estimates, to date, of monthly variations of cloud fractions and the impact of clouds on the surface radiation budget. To determine how well the data collected at Barrow and analyzed in this study represent cloud fraction, surface radiation budget, and cloud radiative forcing in the western Arctic regions, we also compare with other observations. These results should be valuable for advancing our understanding of the cloud-radiation interactions and for enabling climate/forecast modelers to more fully evaluate their simulations over the western Arctic region.

2. Data Sets

[6] Barrow, located at the northernmost location in Alaska, near cryospheric boundaries, has a prevailing east-northeast wind off the Beaufort Sea and is influenced by both extratropical and Arctic synoptic activity [Stone *et al.*, 2002]. It is a representative site to evaluate climate change

in the western Arctic coastal zone [Stone, 1997]. The monthly mean surface temperature ranges from -25°C during January–February to 4°C during July–August with an annual average of -11°C from the 10 year surface observations at both ARM NSA and NOAA BRW sites.

2.1. Cloud Observations

[7] The centerpiece of the ARM cloud-radiation instrument array is the millimeter wavelength cloud radar (MMCR) [Moran *et al.*, 1998; Clothiaux *et al.*, 2000]. The MMCR operates at a wavelength of 8 mm in a vertically pointing mode and provides continuous profiles of radar reflectivity from hydrometeors moving through the narrow radar field of view (FOV), allowing for the identification of clear and cloudy conditions. The micropulse lidar is sensitive to the second moment of the particle distribution (or the cross-sectional area of the particle) unlike the MMCR, which is sensitive to the sixth moment (it detects precipitation-sized or ice particles below cloud base). Thus, the lidar can provide more reliable estimates of cloud-base height and optically thin cirrus cloud properties than the MMCR [Wang and Sassen, 2002]. Therefore, the combined radar-lidar measurements have been used as the best method to estimate cloud fraction (CF) in many studies [e.g., Intrieri *et al.*, 2002a; Dong *et al.*, 2005, 2006a].

[8] For this study, the CF time series are defined by the percentage of returns that are detected as cloudy within a specified sampling period (e.g., month), i.e., the ratio of the number of hours when both radar and lidar detected clouds simultaneously to the total number of hours when all measurements were available (called the radar-lidar method hereafter). The radar-lidar data used in this study are the Mace PI product [Mace *et al.*, 2006], which mimics The Active Remote Sensing of Clouds product [Clothiaux *et al.*, 1999, 2000]. The similarities and differences between two data sets have been discussed in the study by Feng *et al.* [2009]. This study uses approximately 74% of all possible radar-lidar data during the period 1999–2004 (ARM MMCR data were not available after 2004). Although the radar-lidar derived CFs represent only a pencil beam of the sky that depends on the advection of clouds overhead, they have been found to be statistically representative in long-term averages (i.e., monthly) of the entire sky when compared with long-term satellite and surface observations [Dong *et al.*, 2006a; Xi *et al.*, 2010; Kennedy *et al.*, 2010]. Additionally, given the long periods of darkness at higher latitudes that precludes the use of visible instrument methods of cloud amount determination, the radar-lidar method does afford the most viable means of determining CF all year round. The atmospheric precipitable water vapor (PWV) and cloud liquid water path (LWP) are retrieved from the microwave radiometer brightness temperatures measured at 23.8 and 31.4 GHz using a statistical retrieval method [Liljegren *et al.*, 2001]. The root-mean-square (RMS) accuracies of the retrievals are about 20 g m^{-2} and 10% for cloud LWP below and above 200 g m^{-2} , respectively [Dong *et al.*, 2000; Liljegren *et al.*, 2001].

[9] To estimate quantitatively the impact of clouds on the surface radiation budget, we have also processed ARM Vaisala ceilometer data from June 1998 to May 2008 (to match the time period for which we have radiation measurements). The Vaisala ceilometer is an unattended, active remote-sensing device designed to measure the lowest cloud-

Monthly variations of cloud fraction at Barrow, Alaska

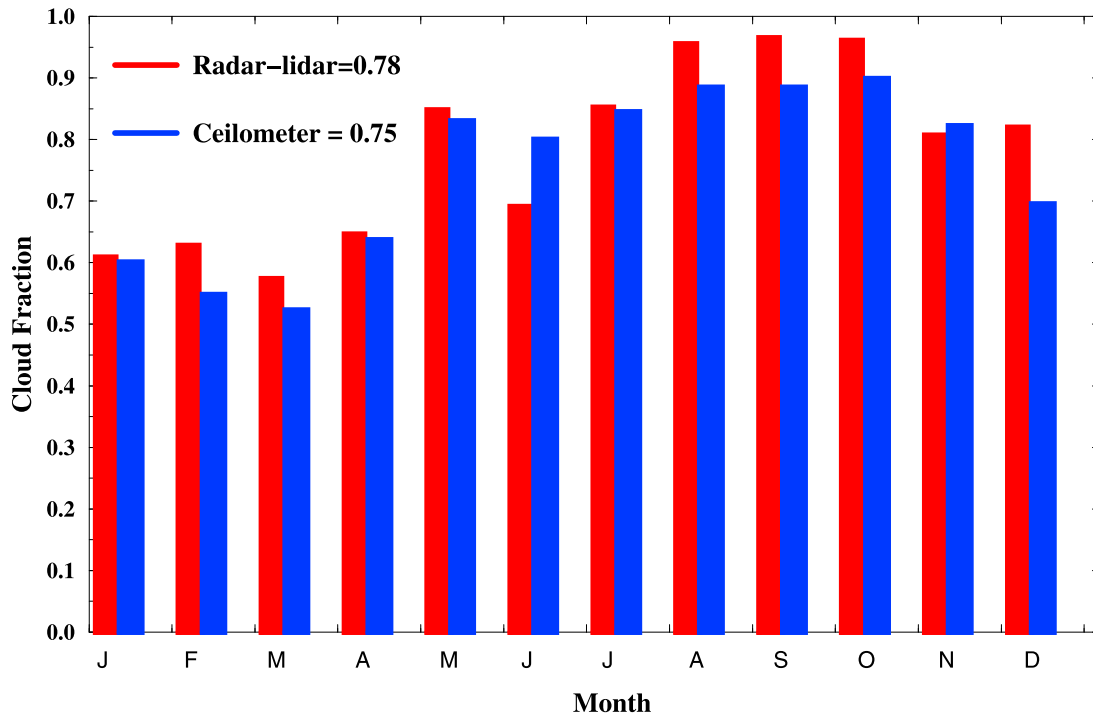


Figure 1. Monthly means of cloud fractions derived from ARM NSA radar-lidar measurements during the period 1999–2004 and ARM NSA ceilometer measurements during the period of June 1998 to May 2008.

base height (H_{base}) up to 7.6 km (may miss some high clouds). The cloud fraction is estimated from the ceilometer-derived cloud bases below 7.6 km using the same method as radar-lidar measurements. During the 10 year period, the ceilometer measurements are available 94.93% of the time. Surface air temperature (T_{sfc}) was also collected where it was measured by the conventional in situ sensors (2 m above ground) mounted on a 10 m tower at the ARM NSA site.

2.2. Radiation Measurements

[10] At the ARM NSA site the up- and down-looking standard Eppley precision spectral pyranometers (PSPs) and precision infrared pyrgeometers (PIRs) in heated ventilators provide measurements of hemispheric downward and upward broadband shortwave (SW, 0.3–3 μm) and longwave (LW, 4–50 μm) fluxes at the surface, respectively. In this study the SW and LW fluxes were collected from June 1998 to May 2008 and quality checked using the QC radiation value added product [Long and Shi, 2008]. Estimates of uncertainties for global SW (measured by unshaded PSPs), total SW-down (the sum of direct and diffuse SW-down fluxes), and LW fluxes are 10, 10, and 4 W m^{-2} , respectively [Long and Shi, 2008]. The global SW fluxes have been corrected for IR loss using the method of Younkin and Long [2003]. The surface albedo (R_{sfc}) is derived from the ratio of upward to downward global SW flux measurements.

[11] BRW, established officially in January 1973 [Geophysical Monitoring for Climatic Change (GMCC), 1974], is located about 8 km northeast of the village of Barrow and less than 1 km northeast of the ARM NSA site.

Both the BRW and ARM sites are located upwind of town, thus influence due to the town's development is minimal [Stone *et al.*, 1996, 2002]. The downward and upward SW and LW fluxes at BRW were also measured using PSPs and PIRs during the period from June 1998 to May 2008. The instruments are calibrated routinely at the Solar Radiation Calibration Facility (SRCF) of NOAA-ESRL in Boulder, Colo. The PSPs agree within 2% of the NOAA SRCF standard reference instruments, which results in absolute errors of $<10 \text{ W m}^{-2}$ for large solar zenith angles and clear-sky conditions and $<7 \text{ W m}^{-2}$ for SW irradiances $>200 \text{ W m}^{-2}$. Routine PIR calibrations produce LW irradiance values within 1% of a blackbody reference cell, which results in absolute errors of $\sim 4 \text{ W m}^{-2}$ [Stone *et al.*, 1996].

[12] Because cloud fraction is generally high over the western Arctic region, we use the empirical curve-fitting technique of Long and Ackerman [2000] to infer clear-sky SW-down flux. The clear-sky SW-up flux is estimated using the technique described in the study by Long [2005], where the clear-sky solar zenith angle dependence of the surface albedo is taken into account, and the clear-sky SW-up flux is estimated by the clear-sky albedo and SW-down flux. The clear-sky broadband effective LW emissivity and LW-down estimation use surface air temperature and relative humidity and fits to detected clear-sky LW-down measurements [Long, 2004; Long and Turner, 2008], an adaptation of the techniques of Marty and Philipona [2000] and Durr and Philipona [2004]. Fit coefficients for cloudy periods are derived by interpolating between clear-sky periods following the method of Long and Ackerman [2000]

Table 1. Seasonal Means of Cloud, Radiation, and Surface Parameters at Barrow, Alaska, During the 10 Year Period: June 1998 to May 2008^a

Parameter	Winter	Spring	Summer	Autumn	Annual
CF (radar)	0.683	0.693	0.820	0.911	0.778
CF (ceilo)	0.615	0.663	0.843	0.869	0.748
LWP (gm^{-2})	33.1	51.6	109.3	98.3	73.0
PWV (cm)	0.371	0.554	1.808	0.834	0.829
H_{base} (km)	1.79	1.77	1.20	1.38	1.53
T_{rad} (K)	233.7	241.2	263.7	253.2	247.9
T_{air} (K)	249.4	257.4	276.1	266.6	262.4
$\text{SW}_{\text{clr}}^{\downarrow}$ (Wm^{-2})	5.4	203.0	300.8	50.0	139.8
$\text{SW}_{\text{clr}}^{\uparrow}$ (Wm^{-2})	4.4	162.6	79.6	14.7	65.3
$\text{LW}_{\text{clr}}^{\downarrow}$ (Wm^{-2})	160.7	184.1	255.0	212.8	203.2
$\text{LW}_{\text{clr}}^{\uparrow}$ (Wm^{-2})	200.3	234.0	346.7	279.9	265.2
$\text{SW}_{\text{all}}^{\downarrow}$ (Wm^{-2})	4.8	165.7	193.3	24.0	96.9
$\text{SW}_{\text{all}}^{\uparrow}$ (Wm^{-2})	3.4	132.6	52.1	6.5	48.6
$\text{LW}_{\text{all}}^{\downarrow}$ (Wm^{-2})	183.9	212.1	301.3	262.5	240.0
$\text{LW}_{\text{all}}^{\uparrow}$ (Wm^{-2})	213.9	245.3	339.3	286.8	271.3
CRF_{SW} (Wm^{-2})	0.3	-7.2	-80.0	-17.7	-26.2
CRF_{LW} (Wm^{-2})	9.6	16.5	53.8	42.8	30.7
CRF_{net} (Wm^{-2})	9.9	9.2	-26.2	25.1	4.5
R_{sfc}	0.857	0.819	0.185	0.335	0.549

^aAll values are averaged from June 1998 to May 2008 except for CF (radar) (January 1999 to December 2004). All values are from ARM NSA observations except for R_{sfc} from NOAA global SW fluxes. Four seasons are defined as winter (December–February), spring (March–May), summer (June–August), and autumn (September–November).

for the SW. Because it is difficult to estimate clear-sky LW-up fluxes using the empirical curve-fitting technique, the monthly mean clear-sky LW-up flux is simply averaged for all clear-sky LW-up flux measurements during that month. Therefore, inferred clear-sky SW and LW fluxes on cloudy days are not actual measurements rather they are derived from the measurements. As such they may be more appropriate than model calculations in estimation of cloud radiative forcing (CRF) because the estimated clear-sky values automatically incorporate any biases between measured and modeled surface downward shortwave fluxes [Kato *et al.*, 1997; Long and Ackerman, 2000].

[13] CRF, the change in the net radiation budget due to clouds [Ramanathan *et al.*, 1989; Dong and Mace, 2003; Dong *et al.*, 2006a], represents the bulk effects of clouds on the net radiation budget. It is a simple but effective means of studying cloud-radiation interactions and diagnosing problems in general circulation models. The CRF is the difference between the net surface fluxes (down minus up) for all-sky conditions of SW and LW (Q_1 and F_1) and for respective clear-sky conditions (Q_0 and F_0), in which $\text{CF} = 0$, defined as

$$\text{CRF}_{\text{SW}} = Q_1 - Q_0 \quad (1a)$$

and

$$\text{CRF}_{\text{LW}} = F_1 - F_0, \quad (1b)$$

respectively. The NET CRF, CRF_{NET} , is the sum of CRF_{SW} and CRF_{LW} at the surface. Positive values of CRF indicate increased radiative flux at the surface due to the presence of clouds and negative values denote a radiative energy loss. Positive and negative forcings lead to warming and cooling tendencies, respectively. The uncertainties of monthly CRFs should be smaller, or at least no more, than the uncertainties of

their flux components ($\sim 10 \text{ Wm}^{-2}$ for SW and 4 Wm^{-2} for LW) because the CRF is calculated from the difference between net all-sky and clear-sky fluxes.

3. Results and Discussions

3.1. Arctic Cloud Fraction

[14] Figure 1 shows monthly time series of cloud fractions (CFs) as derived from the combined ARM radar-lidar measurements (1999–2004) and ARM ceilometer measurements (June 1998 to May 2008) at the ARM NSA site. The annual averaged CFs derived from radar-lidar and ceilometer measurements are 0.78 and 0.75, respectively. In general, CF increases significantly from March to May (0.57→0.84), remains relatively high (~ 0.80 – 0.9) from May to October, and then decreases from November to the following March (0.8→0.57). There are two distinguishable periods with low CF (~ 0.6) from January to April and high CF (~ 0.9) from August to October, respectively. The CFs in other months basically fall within these two periods with a range of CF from 0.7 to 0.8. The seasonal means of CF and other parameters are listed in Table 1.

[15] As discussed in section 2.1, the most viable method to derive year-round CF at Barrow is to use the combined radar-lidar measurements. Although both CFs are derived from different measurements (radar-lidar versus ceilometer) and time periods (1999–2004 versus 1998–2008), they agree quite well in terms of their annual cycle and month-to-month magnitudes. Note that the CFs derived from the ceilometer measurements during the period 1999–2004 are almost the same as those during the period 1998–2008. As shown in Figure 1, the CFs derived from ceilometer measurements are slightly lower than those derived from radar-lidar measurements through the course of the year because the ceilometer might miss some high clouds (when $H_{\text{base}} > 7.6 \text{ km}$), which is beyond the upper limit of ceilometer measurements. The vertical distribution of cloud fraction derived from the 6 year ARM radar-lidar data (not show here) shows that the 3% difference in two CFs indeed represents the percentages of high clouds ($> 7.6 \text{ km}$). However, this cannot explain why the ceilometer-derived CF is higher in June. The radar-lidar derived CF in June is averaged from months of June of 2000, 2003, and 2004 because the radar did not work or only worked for a few days during months of June of 1999, 2001, and 2002. Therefore, the radar-lidar derived CF in June is likely not as statistically representative.

3.2. Surface Radiation Budget

[16] Figure 2 illustrates the monthly mean downward and upward SW and LW fluxes under clear-sky and all-sky conditions using the data collected at the ARM NSA and NOAA BRW sites during the period June 1998 to May 2008. The multiyear monthly means of clear-sky SW and LW fluxes constitute the references herein for studying the impact of clouds on the surface radiation budget (SRB). As shown in Figure 2, the monthly means of estimated clear-sky and measured all-sky SW-down and LW-down fluxes at the two facilities are almost identical. The monthly means of clear-sky SW-down flux are primarily determined by the annual solar cycle and its associated changes in intensity and duration over Northern Alaska. The monthly variations of

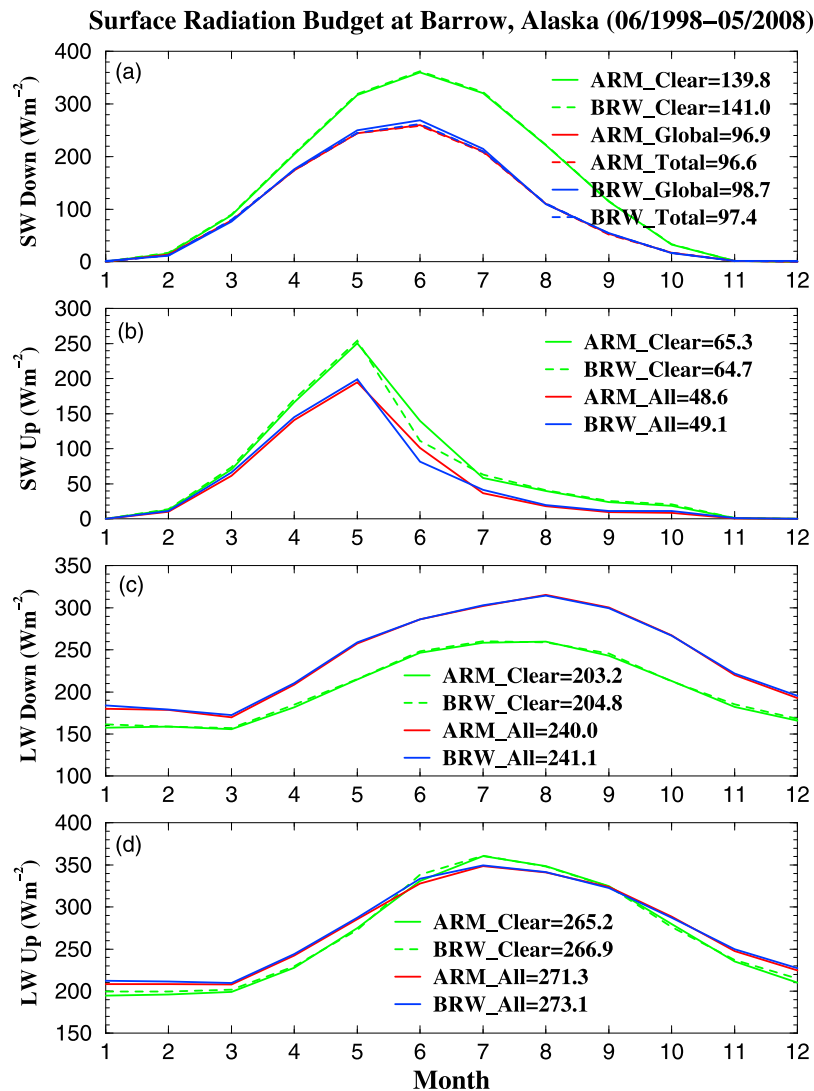


Figure 2. Monthly means of (a) SW-down, (b) SW-up, (c) LW-down, and (d) LW-up fluxes for clear skies and all skies at the ARM NSA and NOAA BRW sites, June 1998 to May 2008. The global SW-down and SW-up fluxes are measured by unshaded PSPs, while the total SW-down flux is the sum of direct and diffuse SW fluxes.

all-sky SW-down flux are skewed slightly from this pattern due to the influence of clouds and aerosols, their optical properties, and the changing surface albedo. The annual mean differences between global and total SW-down fluxes at the ARM NSA and NOAA BRW sites are 0.3 and 1.3 Wm^{-2} , respectively. The ensemble annual all-sky SW-down difference between two sites is only 1.3 Wm^{-2} . These agreements are very encouraging considering the measurements are made independently at locations separated by about 1 km, and instrument calibrations and processing are handled by the individual groups.

[17] The monthly means of all-sky LW-down flux slightly decrease from 180 to 170 Wm^{-2} during January–March, then increase monotonically from March to August, and finally decrease gradually into winter. The all-sky LW-down fluxes are strongly influenced by variations in CF, cloud-base temperature and height [Dong *et al.*, 2006a; Shupe and Intrieri, 2004], and cloud LWP (which will be shown in section 5). The monthly means of clear-sky LW-down flux

mimic their all-sky counterparts at lower magnitude and are primarily determined by the atmospheric temperature profile and PWV as discussed in the study by Dong *et al.* [2006a]. As listed in Table 1, the clear-sky LW-down flux increases 71 Wm^{-2} (184→255 Wm^{-2}) from spring to summer because of the significant increase of PWV (0.554→1.808 cm). The all-sky LW-down flux increases 89 Wm^{-2} (212→301 Wm^{-2}) from Spring to Summer. Therefore, the LW-down differences (28→46 Wm^{-2} from Spring to Summer) between all-sky and clear-sky conditions are mainly due to the significant increases of LWP (51.6→109.3 gm^{-2}) and cloud radiating temperature (241→264 K) and the decrease of cloud-base height (1.77→1.20 km).

[18] Notice that the clear-sky LW-down flux in Figure 2b represents the clear-sky climatology at Barrow, Alaska, and one should be careful when comparing this result with others. For example, the 10 year averaged clear-sky LW-down flux is about 156 Wm^{-2} during March, while it is described as being between 120 and 140 Wm^{-2} during March 2001 by

Marty et al. [2003] because there were only a few clear-sky days with abnormal cold temperatures during March 2001 used in their work.

[19] Although the clear-sky and all-sky SW-up and LW-up fluxes at the two sites are generally in agreement, some issues exist, stemming from the fact that upward fluxes depend on variations in downward flux as well as surface albedo and emissivity. The BRW clear-sky and all-sky SW-up fluxes are nearly identical to ARM results through the course of the year but are much lower ($\sim 20\text{--}30\text{ Wm}^{-2}$) than ARM values in June. The difference in June is most likely due to the timing of snowmelt at the two sites. The ARM site is more prone to drifting around the albedo tower due to the nearby obstructions, whereas the NOAA albedo tower is located in an area that is less prone to drifting. In addition to the building and tower obstructions at the ARM NSA site, there is also a road running through the site that is elevated and sloped to shed drifts. In contrast, the NOAA facility PSPs are in open, level tundra environment. The ARM PSPs are located at 10 m, whereas the NOAA albedo rack stands at only 4 m, affecting the field of view (FOV) of the instrumentation.

[20] The monthly variations of LW-up flux, determined by surface emissivity and temperature, are highly correlated with their downward counterparts, having slightly greater magnitudes that peak during July. As shown in Figure 2d, the all-sky LW-up flux from January to March is nearly constant ($\sim 210\text{ Wm}^{-2}$) because the monthly mean surface air temperatures are also constant ($\sim 25^\circ\text{C}$) during this period. The clear-sky LW-up flux mimics its all-sky counterpart with lower values. From March to July both clear-sky and all-sky LW-up fluxes increase significantly ($200\text{--}360\text{ Wm}^{-2}$) due to increases from both downward SW and LW fluxes, particularly following snowmelt, as well as from surface temperature ($-25^\circ\text{C}\text{--}4^\circ\text{C}$). The clear-sky LW-up fluxes remain consistently lower ($\sim 11\text{ Wm}^{-2}$) than all-sky values during January–May, are nearly the same in June, but about 9 Wm^{-2} higher than all-sky values during July–August, and finally reach equal value in September. During January–May, the 11 Wm^{-2} increases under all-sky conditions represent the warming effect of clouds on the Arctic surface, especially when the LW effect is dominant during that period. During summer (July–August), the LW-up flux during clear-sky conditions is higher than that during all-sky conditions, presumably due to increased absorption of SW radiation at the surface during clear-sky periods when surface albedo is low.

3.3. Cloud Radiative Forcing

[21] The monthly means of SW, LW, and NET CRFs for both ARM and BRW are illustrated in Figure 3. In the CRF calculations, the ARM- and BRW-derived clear-sky fluxes were used as baseline for calculating their CRFs, respectively. The LW CRFs are primarily determined by the differences in LW-down fluxes between all- and clear-sky conditions because the differences between all- and clear-sky LW-up fluxes are small relative to their downward counterparts. The ARM and BRW LW CRFs show excellent agreement, maintain moderate positive values, and vary slightly over the course of the year with an annual average of 30 Wm^{-2} , having a minimum value of $\sim 6\text{ Wm}^{-2}$ in March, increasing monotonically to a maximum of $\sim 63\text{ Wm}^{-2}$ during August. LW

CRF decreases through the winter and early spring when clouds tend to be optically thin and cloud fraction is at a minimum.

[22] Variations in SW CRFs are approximately the inverse of their LW counterparts and have the greatest negative impact during the snow free months of July and August. Because there is essentially no incoming SW radiation during November–January, values of SW CRF are zero during these months and are always negative during sunlit months. As shown in Figure 3a, values of SW CRF slowly decrease from winter to spring, and reach their maximum negative ($\sim -90\text{ Wm}^{-2}$) during July–August when the cooling effect of clouds is greatest and the surface albedo is the lowest. The only difference in calculating global and total SW CRFs is the global and total SW-down fluxes. It is surprising to see the SW CRFs derived from NOAA global flux measurements agree very well with ARM SW CRFs, especially in June because the dips in SW-up flux in both clear and all skies have been cancelled. The more negative SW CRF derived from NOAA total flux measurement during June is due to lower total SW-down flux ($\sim 7\text{ Wm}^{-2}$) than NOAA global SW-down flux. The annual average SW CRF is approximately -27 Wm^{-2} on the basis of the combined ARM and BRW analysis.

[23] The monthly variations of NET CRFs, the sum of SW and LW CRFs, generally follow the cycle of SW CRFs but have values modified by LW CRFs. On annual average, the negative SW CRFs and positive LW CRFs nearly cancel. The annual average NET CRF is about 3.5 Wm^{-2} on the basis of the combined ARM and BRW analysis. The results indicate that clouds in Barrow have a net warming effect on the surface throughout most of the year but have a net cooling effect on the surface during the period from mid June to mid September where the surface is free of snow.

3.4. Uncertainties in CRFs

[24] In this study the CRF is determined by the difference between the net surface fluxes during all-sky and clear-sky conditions. In fact, the CRF should be the difference between the net surface fluxes under all-sky condition and the clear-sky values during all-sky condition. Because it is impossible to measure clear-sky fluxes under all-sky condition, the clear-sky values are either estimated from the empirical curve fitting of clear-sky measurements [*Dong et al.*, 2006a and this study] or calculated from the radiative transfer model [*Intrieri et al.*, 2002b, and *Shupe and Intrieri*, 2004]. Neither method can fully represent the ground truth clear-sky fluxes under all-sky condition. The estimated clear-sky fluxes from observational data may be slightly different from the ground-true clear-sky values because clear skies are typically drier than all skies. On the other hand, model calculations may result in biases between observations and calculations as pointed out in the studies by *Kato et al.* [1997] and *Long and Ackerman* [2000].

[25] To understand the uncertainties in calculating CRFs due to different surface and sky backgrounds, *Dong et al.* [2006a] estimated the uncertainties of CRFs due to the different surface albedos and LW-up fluxes, and SW-down and LW-down fluxes resulted from different atmospheric water vapor values under the clear-sky and cloudy conditions. *Dong et al.* [2006a] parameterized the clear-sky downward LW and SW fluxes as a logarithmic function of

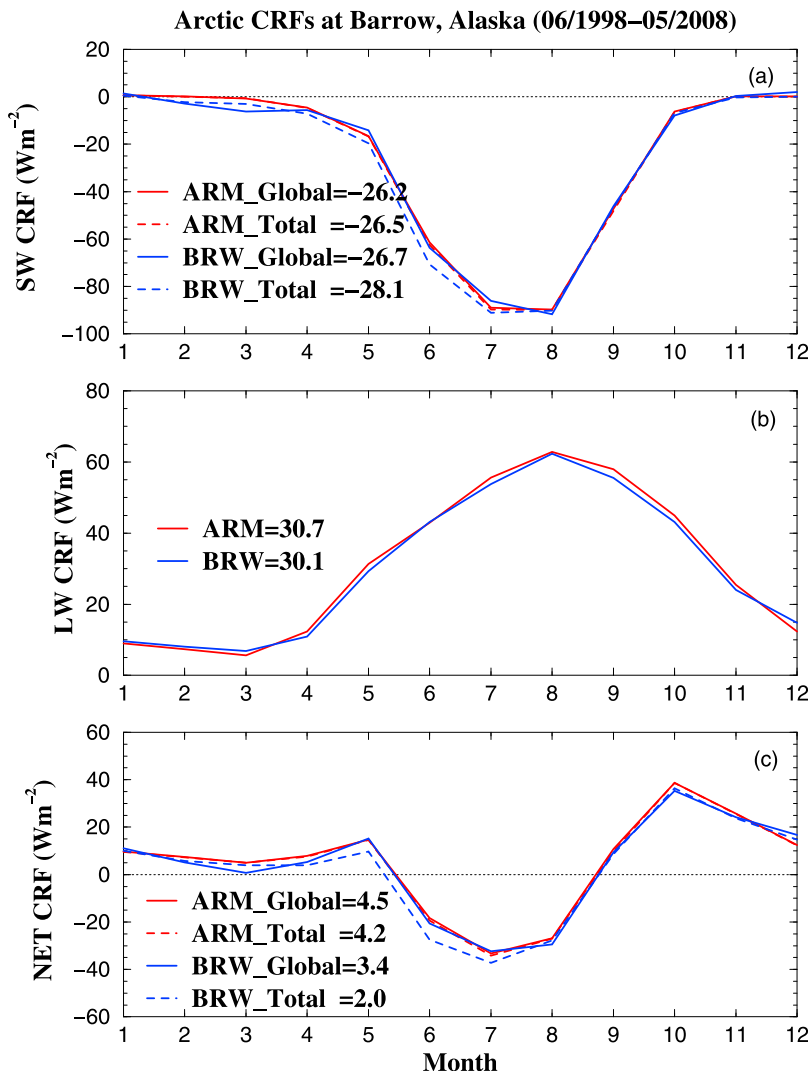


Figure 3. Monthly means of all-sky (a) SW, (b) LW, and (c) NET cloud radiative forcings (CRFs) at the ARM NSA and NOAA BRW sites, June 1998 to May 2008. The clear-sky SW-down and up, and LW-down values were estimated using the empirical fitting techniques, and LW-up values are averaged all clear-sky LW-up measurements during the 10 year period.

PWV based on the 6 year ARM Southern Great Plains (SGP) data set and found that the downward SW flux decreases and LW flux increases (dominant) with increasing PWV. Although we cannot quantitatively estimate the uncertainties of CRFs due to different atmospheric PWV values under the clear-sky and all-sky conditions over Barrow, the uncertainties of CRFs in this study should be similar to, or with lower magnitudes than, those in the study by Dong *et al.* [2006a].

[26] Another possible uncertainty in calculating SW and LW CRFs is the inferred clear-sky SW-down flux using the empirical curve-fitting technique of Long and Ackerman [2000] and estimated clear-sky LW-down flux using the method by Long and Turner [2008]. Because cloud fraction is generally high over the western Arctic region, it is difficult to use a few days of clear-sky SW flux measurements, especially during the spring transition period with low solar elevation angle and higher surface albedo, to represent the true monthly mean values. However, with a total of 10 years of

observations and relatively small variation in LW flux, is it possible to determine the monthly means of clear-sky LW-down flux from only a few days of clear-sky measurements? To answer this question, we produced Figure 4. As illustrated in Figure 4a, although the overall means are nearly the same (203.2 versus 204.4 Wm^{-2}) between the Long and Turner [2008] derived and measurement-only aggregates, there are relatively large differences from winter to summer from the 10 year overall monthly averages. If we used the monthly mean values calculated only from the clear-sky LW-down measurements, it would slightly increase LW CRFs during winter ($+8 \text{ Wm}^{-2}$) but significantly decrease LW CRFs during July–August ($\sim -17 \text{ Wm}^{-2}$), and the difference in LW CRFs between winter and summer would be smaller than our current results. However, the uncertainties of monthly means from the measurement-only are much larger for each individual month as shown in Figure 4b, especially during the summer months because there are less clear-sky days during the summer months, and thus they are less representative of

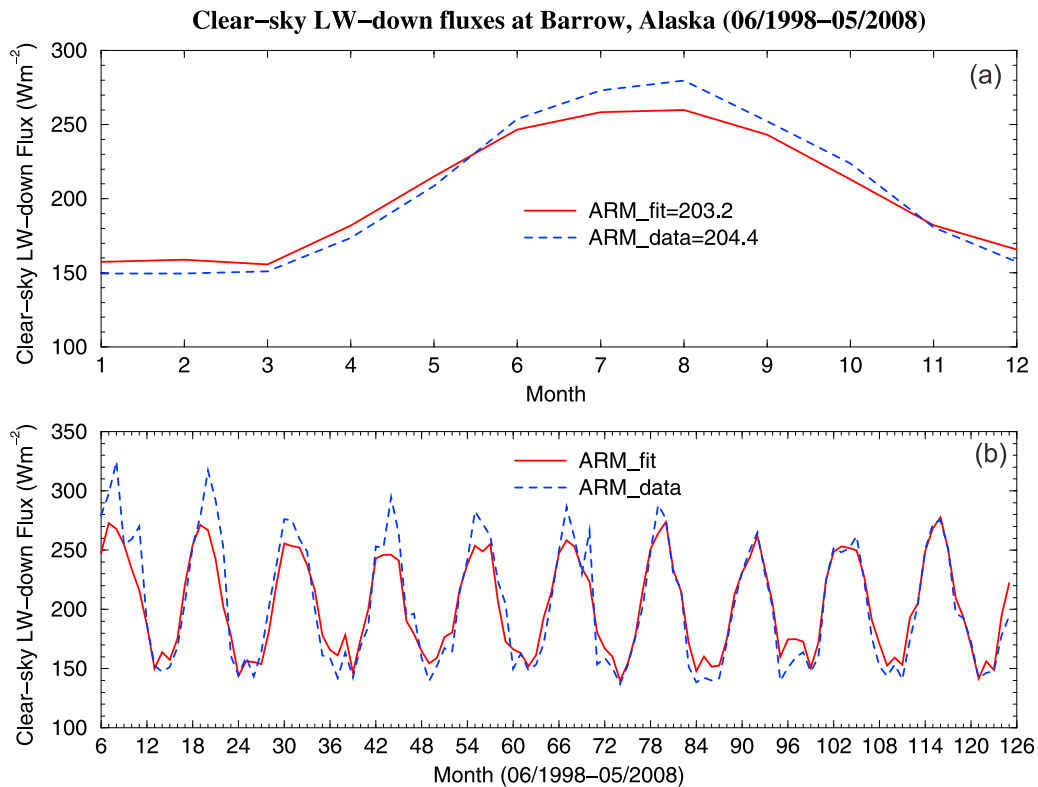


Figure 4. (a) Monthly means of clear-sky LW-down flux calculated from the derivation (solid line) and measurement-only (dashed line) at the ARM NSA site during the 10 year period. (b) Same as Figure 4a except for each individual month from June 1998 to May 2008.

the entire month. As demonstrated in Figure 4b, the summer LW-down monthly means calculated from the measurement-only range from 250 to 330 Wm^{-2} , which is beyond the natural LW-down variation. Yet those from the methodology by Long and Turner [2008] fall in a range of 250–280 Wm^{-2} , which is what is expected. Further inspection shows that there are 22 months with less than 5 days of clear skies (out of 120 months), including 7 months during the period July–August. Therefore, the monthly means calculated from the derivations are consistent from winter to summer, and more representative of the entire month of clear-sky information than the measurement-only, especially for individual months and during summer months.

3.5. The 10 Year Trends/Tendencies

[27] The global average surface temperature has increased by about 0.6°C–0.7°C since the mid-1960s [Kennedy *et al.*, 2007], and the corresponding temperature over the Arctic region (north of 60°) has raised 1.9°C–2.0°C [Richter-Menge *et al.*, 2008]. At Barrow, Alaska, the average temperature has increased 1.9°C during the period 1949–2005 with the maximal increase during the winter and spring seasons (3.2°C and 2.5°C) and the minimal increase during the summer and autumn seasons (1.5°C and 0.83°C) using the measurements at the National Weather Service (NWS) station in the town of Barrow, which is about 7 km from the ARM NSA site [Shulski and Wendler, 2007]. Therefore, it is natural to investigate these climate changes and their associated changes in CF and SRB over Barrow, Alaska, using the ARM data set during the 10 year period.

[28] To determine if the Barrow warming occurs year round or during particular seasons, we plot the seasonal averages of T_{air} , CF, all-sky SW-down, and LW-down fluxes from 1998 to 2008 in Figure 5. Linear regression analyses are performed on each parameter to detect any significant trends or tendencies during the 10 year period using the Student's t test. Here trends are defined as statistically significant when the confidence level (CL) > 90%. On the other hand, temporal changes with a CL < 80% (i.e., not statistically significant trends) are simply considered tendencies. The decadal changes for these four parameters for each season and year round, as well as their CL values are listed in Table 2. The indicated year-round change in T_{air} is 1.07°C, i.e., a 1.07°C warming over the 10 year period, which is mostly due to increases during the autumn (1.9°C) and winter (1.75°C) seasons. Notice that the tendencies toward increased temperatures during autumn and winter seasons found in this study are different from the maximal increase during the winter and spring seasons found in the study by Shulski and Wendler [2007]. The difference may be due to the different locations (~7 km apart) and different time periods (1949–2005 versus 1998–2008). To further confirm that point, we used the NWS observed T_{air} during the period from June 1998 to May 2008 and performed linear regressions where the temperature tendencies during autumn and winter seasons are nearly identical to those derived from ARM observations, but its temperature increases 1.5°C during spring season. The regressions, however, result in CL < 80%, indicating that the 10 year

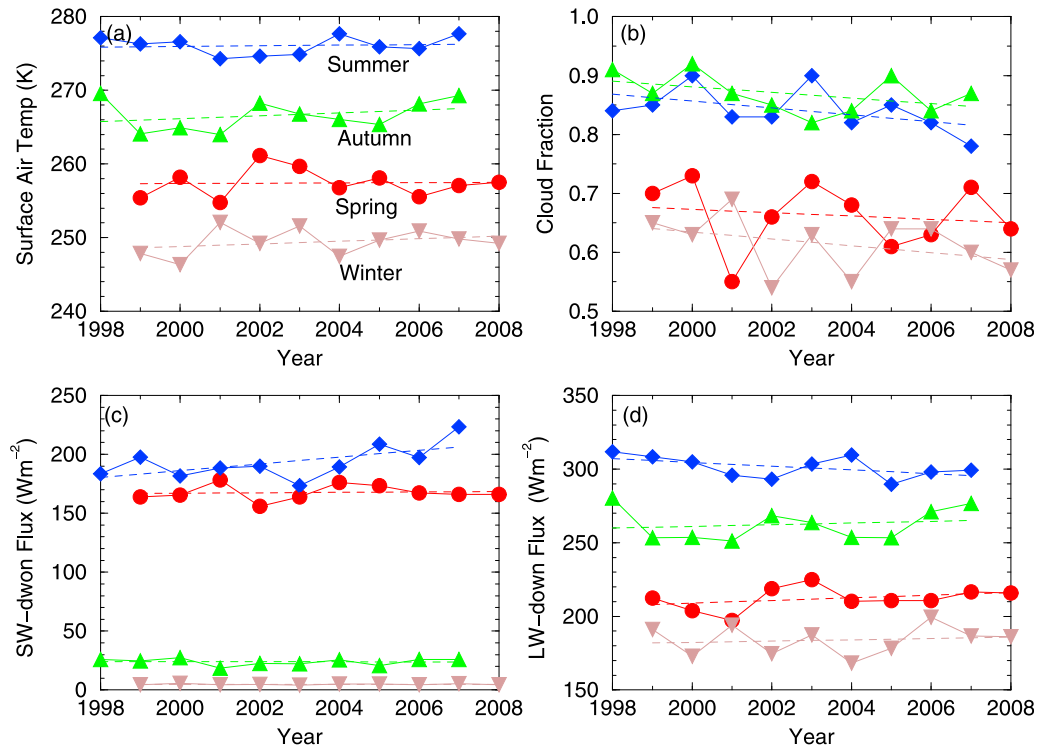


Figure 5. Seasonal means of (a) surface air temperature, (b) ceilometer-derived cloud fraction, and all-sky (c) SW-down and (d) LW-down fluxes at the ARM NSA site from June 1998 to May 2008. Four seasons are defined as winter (December–February), spring (March–May), summer (June–August), and autumn (September–November).

period is too short to reveal statistically significant trends in this parameter.

[29] For the 10 year period, statistically significant trends (CL > 92%) have been detected during the summer season where the CF decreases 0.06, resulting in an increase of 28.8 Wm^{-2} in SW-down flux and a reduction of 12.7 Wm^{-2} in LW-down flux. This result makes physical sense because all-sky insolation normally increases and LW-down flux decreases with decreased CF. This result is also consistent with the study by Dong *et al.* [2006b] at the ARM Southern Great Plains (SGP) site. The year-round tendencies in CF, SW-down, and LW-down fluxes are -0.048 , 6.0 , and 1.54 Wm^{-2} , during the 10 year period. The inability to identify statistically significant trends in year-round and other seasons are either due to the short period (10 years), the highly variable surface albedo and complex environmental conditions at Barrow, or the lack of an actual trend in a given parameter. In summary, the recent decadal temperature rise at Barrow can be characterized by tendencies of warming during periods of low solar illumination or darkness, mainly during autumn and winter months. To some extent, temperature variations are associated with changes in CF and downward SW and LW fluxes.

4. Comparisons With Other Data Sets

[30] To determine how well the data collected at Barrow and analyzed in this study represent CF, SRB, and CRF in the western Arctic region, it is necessary to compare with other observations. Therefore, we compare the CFs in this

study with the ground-based observations at the ARM NSA site (May–September 2000) [Dong and Mace, 2003], during the SHEBA field experiment (from 75.3°N , 142.7°W to 80.5°N , 166°W during October 1997 to October 1998) [Intrieri *et al.*, 2002a, 2002b]; and the Moderate Resolution Imaging Spectroradiometer (MODIS) and CloudSat/Cloud-Aerosol Lidar and Infrared Pathfinder Satellite Observation (CALIPSO) satellite retrievals over the western Arctic region (120°W – 180°W , 70°N – 90°N) [Kay *et al.*, 2008]. We also compare with the CF and SRB derived from advanced very high resolution radiometer (AVHRR) data set from 1982 to 1999 over the western and entire Arctic regions [Wang and Key, 2005]. Although these comparisons are based on data collected at different locations and years, it is instructive to consider the similarities and differences between the ARM NSA and NOAA BRW results at a single

Table 2. Seasonal Changes of Surface Air Temperature, Cloud Fraction, All-Sky SW-Down and LW-Down Fluxes During the 10 Year Period at the ARM NSA Site^a

Season	T_{site} (K)		CF		SW^{\downarrow} (Wm^{-2})		LW^{\downarrow} (Wm^{-2})	
	ΔT	CL	ΔCF	CL	$\Delta\text{SW}^{\downarrow}$	CL	$\Delta\text{LW}^{\downarrow}$	CL
Spring	-0.19	NS	-0.024	NS	-4.3	NS	8.9	NS
Summer	0.4	NS	-0.06	92%	28.8	97%	-12.7	94%
Autumn	1.9	NS	-0.048	90%	-0.2	NS	5.7	NS
Winter	1.75	NS	-0.054	NS	-0.2	NS	4.3	NS
Year	1.07	NS	-0.048	NS	6.0	NS	1.54	NS

^aCL, confidence level; NS, not significant (NS < 80%).

Table 3. Seasonal Means of Cloud Fractions Derived From ARM Radar-Lidar, Ceilometer, SHEBA Radar-Lidar, MODIS, CloudSat-CALIPSO, and AVHRR^a

Location	Data	Source	Winter	Spring	Summer	Autumn	Annual
ARM NSA	Radar-lidar	This study	0.683	0.693	0.820	0.911	0.778
ARM NSA	Ceilometer	This study	0.615	0.663	0.843	0.869	0.748
SHEBA	Radar-lidar	<i>Intrieri et al.</i> [2002a]	0.580	0.869	0.922	0.884	0.814
Western Arctic	MODIS, Terra	<i>Kay et al.</i> [2008]			0.595		
Western Arctic	MODIS, Aqua	<i>Kay et al.</i> [2008]			0.592		
Western Arctic	CloudSat-CALIPSO	<i>Kay et al.</i> [2008]			0.695		
Alaska, 60°N+	AVHRR	<i>Wang and Key</i> [2005]	0.58	0.66	0.71	0.67	0.655
Beaufort Sea	AVHRR	<i>Wang and Key</i> [2005]	0.65	0.53	0.74	0.77	0.673
Canada Basin	AVHRR	<i>Wang and Key</i> [2005]	0.65	0.59	0.81	0.77	0.705
Arctic region 60 N+	AVHRR	<i>Wang and Key</i> [2005]	0.64	0.61	0.74	0.72	0.678

^aThe SHEBA field experiment covered from 75.3°N, 142.7°W to 80.5°N, 166°W during October 1997 to October 1998. The CFs derived from MODIS on Terra are averaged from the summers of 2000–2007, on Aqua from 2003–2007, and on CloudSat-CALIPSO from the summers of 2006–2007 over the western Arctic region (120°W–180°W, 70°N–90°N) in the *Kay et al.* [2008] study. The CFs derived from AVHRR are averaged from 1982 to 1999 over the western and entire Arctic regions [*Wang and Key*, 2005].

location and other data sets collected over the western and entire Arctic regions.

4.1. Cloud Fraction

[31] The cloud fractions derived from ground-based and satellite remote sensors have been defined in our previous studies [*Dong and Mace*, 2003; *Dong et al.*, 2005; *Kennedy et al.*, 2010; *Xi et al.*, 2010] and in section 2.1 of this study. The seasonal means of CFs derived from this study and other studies are listed in Table 3.

[32] The method, data, and location used to derive the monthly mean CF in the study by *Dong and Mace* [2003] are the same as in this study. In the study by *Dong and Mace* [2003], a record of single-layer and overcast low-level Arctic stratus cloud properties has been generated using data collected from May to September 2000 at the ARM NSA site. The record includes liquid-phase and liquid dominant mixed-phase Arctic stratus macrophysical, microphysical, and radiative properties, as well as surface radiation budget and cloud radiative forcing. The monthly CF variation given by *Dong and Mace* [2003] for that period is the same as that in Figure 1, with an average CF of 0.86, which is identical to those derived from radar-lidar measurements (1999–2004) and ceilometer measurements (1998–2008) in this study. As listed in Table 3, the CFs derived from the SHEBA radar-lidar pair during autumn and winter are lower than the ARM radar-lidar pair; however, the CFs during spring and summer are much higher. The CF during spring is more than 0.18 higher than that in this study, which results in 0.04 more clouds on the annual basis. Further, comparing the SHEBA CF during January–September 1998 with the available ARM ceilometer measurements at the ARM NSA site, the averaged CFs are 0.83 and 0.80, respectively.

[33] To study the contribution of cloud and radiation anomalies to the 2007 Arctic sea ice extent minimum, *Kay et al.* [2008] estimated the summer CFs from daytime MODIS observations on Terra from 2000 to 2007, on Aqua from 2003 to 2007, and from CloudSat-CALIPSO radar-lidar observations during 2006–2007. Their corresponding averaged CFs are 0.595, 0.592, and 0.695, respectively. Compared with the summer CFs of this study, the MODIS-derived CFs are about 0.24 lower, indicating that the determination of Arctic cloudiness using current passive

satellite observations still encounters significant obstacles. If we only compare the summers of 2006 and 2007, the averaged CFs from MODIS, CloudSat-CALIPSO, and ARM NSA ceilometer measurements in this study are 0.54, 0.696, and 0.805, respectively.

[34] To further determine the comparative representativeness of the results in this study, we also compare the CFs derived from AVHRR data over the western Arctic region, such as Alaska, the Beaufort Sea, and the Canada Basin, as well as over entire Arctic region from the study by *Wang and Key* [2005]. As presented in Table 3, the CFs derived from AVHRR data increase significantly from spring to summer at lower magnitudes than those in this study with annual differences of ~ 0.07 – 0.1 . More important, the CF values in the study by *Wang and Key* [2005] show an increase from Alaska to the Beaufort Sea and Canada Basin, which is similar to our comparison with the SHEBA results. In addition, the seasonal and annual means of CF over the Beaufort Sea are close to those over the entire Arctic region.

[35] The CFs presented in Figure 1 are comparable to other cloud climatologies produced for the western Arctic region, e.g., those derived from ground-based radar-lidar observations during the SHEBA experiment and from satellite observations made over the western Arctic region. The cloud fractions increase northward based on the comparison with the SHEBA results and those in the study by *Wang and Key* [2005]. The comparisons in Table 3 also suggest that improvements in deriving cloud fractions over Arctic region from current passive satellites, even active sensors on satellites, are required.

4.2. Surface Radiation Budget and Cloud Radiative Forcing

[36] The monthly means of SW and LW fluxes and their derived CRFs in the study by *Dong and Mace* [2003] are based on only the daytime observations ($\mu_0 > 0.2$, the cosine of solar zenith angle), and their values (both positive and negative) are much larger than those in this study. Therefore, we cannot compare the results in these two studies. The monthly variation of all-sky SW-down flux from the SHEBA [*Intrieri et al.*, 2002b] is similar to that in this study with a peak of 282 Wm^{-2} in June, which is about 20 Wm^{-2} higher than the maximum value of this study presumably due to the higher surface albedo during SHEBA ($R_{\text{sfc}} \sim 0.5$) than at the

Table 4. Annual Means of All-Sky LW-Down, SW-Down, and CRFs

Location	Data	LW [↓]	SW [↓]	CRF _{LW}	CRF _{SW}	CRF _{net}
ARM NSA	PSP, PIR	240.0	96.9	30.7	-26.2	4.5
SHEBA	PSP, PIR	229.5	98.4	37.7	-11.0	26.9
Alaska, 60°N+	AVHRR	252.7	301.8	31.3	-49.2	-17.9
Beaufort Sea	AVHRR	214.7	251.7	27.7	-15.3	12.2
Canada Basin	AVHRR	208.6	170.1	29.2	-14.2	15.0
Arctic region, 60°N+	AVHRR	241.2	247.6	35.1	-49.5	-14.4

ARM NSA site ($R_{\text{sf}} \sim 0.2$) during this period. The measured SW-down flux at the surface is higher under high surface albedos than the normal value due to multiple reflections of solar radiation between the cloud layer and the highly reflective surface. The monthly variation of LW-down flux from the SHEBA also mimics the variation of this study with almost the same minimum value ($\sim 160 \text{ Wm}^{-2}$) during winter and slightly lower maximum value ($\sim 294 \text{ Wm}^{-2}$) during summer.

[37] The ARM and NOAA LW CRFs have a minimum value of $\sim 6 \text{ Wm}^{-2}$ in March and a maximum of $\sim 63 \text{ Wm}^{-2}$ during August with the annual average of 30 Wm^{-2} . Although the monthly variations of LW CRF during the SHEBA experiment are nearly the same as those derived from this study, they exhibit a slightly larger seasonal variation because the ARM and NOAA LW CRFs are averaged from a total of 10 years of observations, while the LW CRFs from SHEBA are only over a 1 year period. The maximum negative SW CRF at the ARM NSA ($\sim 90 \text{ Wm}^{-2}$) is much larger than that during the SHEBA experiment ($\sim 53 \text{ Wm}^{-2}$). Comparing the net CRF at the ARM NSA site with that at the SHEBA ship, the summer cooling period is much longer (3 months versus 1–2 weeks), and the summer cooling magnitude is much larger (-34 versus -7 Wm^{-2}). However, the annual net CRF at the SHEBA ship is much larger than that at the ARM site, as listed in Table 4 because the LW warming effect is dominant through most of the year. Notice that this comparison is based on the 5° – 9° latitude difference between the SHEBA ship (76°N – 80°N) and ARM NSA site (71°N). The primary difference in net CRFs at the two sites are due to the much higher surface albedo and solar zenith angle at the SHEBA ship causing the SW CRF to dominate the LW CRF for a short portion of the year than at the ARM NSA site.

[38] To provide additional support to the above argument, we list the LW-down, SW-down, SW/LW/NET CRFs from the Alaska region to the Canada Basin, as well as over the entire Arctic region derived from AVHRR data in the study by Wang and Key [2005]. As listed in Table 4, the annual averaged LW-down fluxes decrease significantly from Alaska to the Beaufort Sea but only a few Wm^{-2} of reduction from the Beaufort Sea to the Canada Basin. The annual averaged LW CRFs over the western and entire Arctic regions are close to those at the ARM NSA and the SHEBA ship. This good agreement suggests that the long-term surface LW CRFs can be accurately derived from satellite observations even with only two overpasses (both local solar times of 0400 and 1400 from AVHRR). The good agreement also indicates that LW CRF does not change over Arctic regions significantly.

[39] The large difference in SW fluxes between this study and that of Wang and Key [2005] is due to the one SW sample

used in their study at the local solar time of 1400 being close to the daily maximum. The most important message from their study is that the cooling effects of SW CRFs from Alaska to the Beaufort Sea are reduced dramatically and nearly identical from the Beaufort Sea to the Canada Basin. The annual averaged NET CRFs change from negative to positive from Alaska to the Beaufort Sea, indicating that Barrow is at or near a critical latitude for neutral NET CRF, where LW CRF and SW CRF are nearly cancelled on the annual basis. That is, with increased distance south of Barrow, the annual SW cooling effect becomes dominant, and the cooling period and strength increases. Conversely, with increasing distance north of Barrow, the LW warming effect becomes more and more important than the SW cooling effect. The latitude of neutral NET CRF is also dependent on latitudinal variations in surface albedo.

5. Sensitivities of CRF to Cloud and Surface Parameters

[40] To quantify the impact of cloud fraction on the SRB, Dong *et al.* [2006a] used 72 monthly mean LW and SW CRFs and their corresponding monthly mean CFs at the ARM SGP site and found that LW CRFs increase and SW CRFs decrease with increasing CF. CRF represents the bulk effects of the seasonal variations of cloud and surface parameters, that is, the surface CRF does not solely represent the radiative effect of clouds, but rather the mixed effects of changes of cloud and surface (atmosphere) properties. The empirical relationships between CRF and CF in the study by Dong *et al.* [2006a] may well represent the radiative effect of changes in cloud properties because the surface (atmosphere) is generally less critical in environments where the variations of the clear-sky fluxes are relatively small compared to the cloud-induced changes. However, the radiative effect due to the seasonal variations of surface parameters, such as surface albedo, in the Arctic are nearly as large as the cloud-induced radiative effect. In other words, the annual CRF would vary significantly even if the cloud properties were constant over the annual cycle in the Arctic. Therefore, it is necessary to investigate the sensitivities of CRF to cloud properties (CF, LWP, cloud radiating temperature, and cloud-base height) and surface albedo in this study.

[41] To investigate the relationships between LW CRFs and cloud properties, the 120 (10 years \times 12 month) monthly mean values have been used and plotted in Figure 6. As shown in Figure 6a, LW CRF increases with increasing CF. This relationship is very similar to those found at the SGP by Dong *et al.* [2006a] and at SHEBA by Shupe and Intrieri [2004]. The similar relationship between all-sky LW CRF and CF at the SGP, NSA, and SHEBA sites indicates that CF plays an important role in determining LW CRF at both middle latitudes and Arctic regions. LW CRF has a strong positive correlation (0.90) with cloud radiating temperature and moderate negative correlation (-0.68) with cloud-base height. These relationships make physical sense because the all-sky LW-down flux is proportional to the cloud radiating temperature, while the cloud radiating temperature decreases with increasing cloud-base height. The relative large mean residual values to the fittings presented in Figure 6 indicate

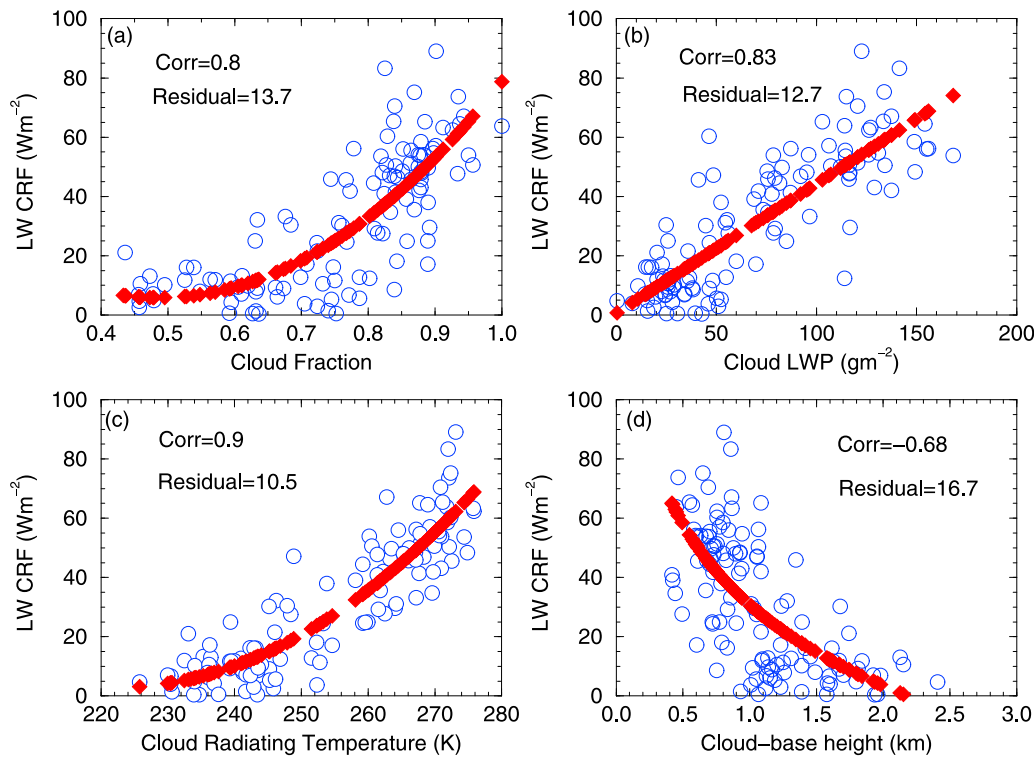


Figure 6. Dependence of all-sky LW CRFs on (a) cloud fraction (derived from ARM ceilometer measurements), (b) cloud LWP (retrieved from ARM microwave radiometer measurements), (c) cloud radiating temperature, and (d) cloud-base height (measured by ARM ceilometer) at Barrow, Alaska, from June 1998 to May 2008.

that the empirical curve fittings are not very significant even though their correlations are high.

[42] To understand the importance of cloud optical depth to LW CRF, we use LWP as a surrogate for optical depth because LWP was directly retrieved from ARM microwave radiometer-measured brightness temperatures. As illustrated in Figure 6b, LW CRF linearly increases with increasing cloud LWP with a strong positive correlation of 0.83. The relationship exhibited in Figure 6b characterizes a number of co-varying parameters. As demonstrated by *Shupe and Intrieri* [2004] and others, LWP should have no further direct impact on LW radiation for $\text{LWP} > 30\text{--}50 \text{ gm}^{-2}$ because clouds essentially emit as blackbodies. The continued apparent sensitivity shown in Figure 6b for higher LWPs is due to related increases in the cloud radiating temperature as the LWP increases in the summer or some factors are not yet entirely understood under the complicated environment at Barrow, Alaska.

[43] Notice that CF increases from 0.52 to 0.89, while LW CRF increases from 6 to 63 Wm^{-2} from March to August. LW CRF represents the bulk integrated effects of the seasonal variations of cloud, surface, and atmospheric parameters, that is, the LW CRF at the surface does not only change with CF only but also other parameters as well. As illustrated in Figure 6, LW CRF increases exponentially with increased CF and cloud radiating temperature and linearly with cloud LWP. In addition to the seasonal variation in cloud properties themselves, there are also the significant differences in aerosol loading, atmospheric profiles of temperature and water vapor, and surface background

between spring and summer. Therefore, more study is required to quantitatively understand the relationship between LW CRF and cloud and surface parameters, as well as atmospheric background.

[44] The sensitivities of SW CRFs to cloud and surface properties are complicated and show much more scattered relationships than those in Figure 6 (not shown here) with slightly lower correlations. A strong positive correlation (0.87) between SW CRF and surface albedo exists because SW CRF values are slightly negative for high R_{sfc} and largely negative for low R_{sfc} . As mentioned above, the SW CRFs calculated in this study represent the mixed effects of seasonal changes of cloud and surface properties, especially under highly varying R_{sfc} through the course of the year. For example, the R_{sfc} over the ARM NSA site has a range of 0.15–0.85 from summer to winter and the monthly mean μ_0 values vary from 0 to 0.37 from winter to summer. The highly varying R_{sfc} and solar zenith angle are the major obstacles in finding the explicit relationships between SW CRFs and cloud and surface properties in this study. To investigate the mixed effects of seasonal changes in cloud and surface properties, we should use a radiative transfer model to calculate the cloud and surface radiative effects, respectively.

6. Summary and Concluding Remarks

[45] We have generated a 10 year record of Arctic CF, SRB, and CRF using ground-based measurements taken at the ARM NSA and NOAA BRW sites between June 1998

and May 2008. This comprehensive data set was used to examine the seasonal variations of Barrow cloudiness and their impacts on the SRB. To determine how well the data collected at Barrow and analyzed in this study represent CF, SRB, and CRF in the western Arctic regions, we also compare with other observations. Finally, we investigate the dependence of SW and LW CRFs on cloud and surface properties. On the basis of our 10 year data analysis and comparisons with other studies, we reached the following conclusions:

[46] 1. The annual averaged CFs derived from the radar-lidar and ceilometer measurements at the ARM NSA site are 0.78 and 0.75, respectively. The CFs increase significantly from March to May (0.57→0.84), remain relatively high (~0.80–0.9) from May to October, and then decrease from November to the following March (0.8→0.57). These CFs are comparable to those derived from ground-based radar-lidar observations during SHEBA and from satellite observations, which show a northward increase over the western Arctic.

[47] 2. The monthly means of estimated clear-sky and measured all-sky SW-down and LW-down fluxes at the two facilities are almost identical with the annual mean differences less than 1.6 Wm^{-2} . This agreement is very encouraging considering the measurements are made independently at locations separated by about 1 km and calibration and processing are handled by different groups. The monthly variation of all-sky SW-down flux from SHEBA is similar to that in this study with a peak of 282 Wm^{-2} in June, which is about 20 Wm^{-2} higher than the maximum value of this study presumably due to the higher surface albedo during SHEBA (~0.5) than at the ARM NSA site (~0.2). The monthly variation of LW-down flux from SHEBA also mimics the variation of this study with almost the same winter minimum value and slightly lower summer maximum value.

[48] 3. Values of LW CRF are at a minimum (6 Wm^{-2}) in March, then increase monotonically to reach a maximum (63 Wm^{-2}) in August, then decrease continuously to the following March. The cycle of SW CRF mirrors its LW counterpart with the greatest negative impact occurring during the snow-free months of July and August. The monthly variations of NET CRF generally follow the cycle of SW CRF, modulated by LW effects. On annual average, the negative SW CRFs and positive LW CRFs nearly cancel, resulting in annual average NET CRF of about 3.5 Wm^{-2} on the basis of the combined ARM and BRW analysis. By including information from other studies, we find that LW CRF does not change significantly over Arctic regions. However, the NET CRF changes from negative at regions south of Barrow to positive at regions in the Beaufort Sea, indicating that Barrow is at or near a critical latitude for neutral NET CRF. That is, with increased distance south of Barrow, the SW cooling effect becomes dominant, and the summer cooling period and strength increase. Conversely, with increasing distance north of Barrow, the LW warming effect becomes relatively more important than the SW cooling effect. The latitude of neutral NET CRF is also dependent on latitudinal variations in surface albedo.

[49] 4. Monthly mean values are used to investigate the sensitivities of LW and SW CRFs to cloud and surface parameters. Empirical relationships between LW CRF and cloud and surface properties show that LW CRF increases

with increasing CF, LWP, cloud radiating temperature with high positive correlations (0.8–0.9). The sensitivities of SW CRFs to cloud and surface properties, however, are complicated by the seasonal changing of Sun angle and highly reflective surface. A strong positive correlation between SW CRF and surface albedo exists. Because the SW CRFs calculated in this study represent the mixed effects of seasonal changes in cloud and surface properties, it is necessary to further investigate the radiative effects of cloud and surface properties with the help of radiative transfer model calculations.

[50] These results can serve as a baseline for studying Arctic cloud fractions and their impact on the radiation budgets at the surface and in the atmosphere when combined with satellite measurements of the top-of-atmosphere fluxes and can serve as ground truth for validating satellite retrievals over Barrow. This 10 year data set over Barrow, Alaska, should also provide statistically reliable estimates of the monthly variations of CF, SRB, and CRF for climate modelers to verify their model simulations.

[51] **Acknowledgments.** We would like to thank Sally Benson and Gerald G. Mace of the University of Utah for providing preprocessed ARM radar-lidar data. This research was primarily supported by NASA NEWS project under grant NNX07AW05G at the University of North Dakota. The University of North Dakota authors were also supported by NSF under grant ATM0649549, the NASA CERES project under grant NNL04AA11G, and the NASA MAP project under grant NNG06GB59G. Long and Shupe acknowledge the support of the Climate Change Research Division of the U.S. Department of Energy as part of the Atmospheric Radiation Measurement (ARM) Program. R. Stone receives support from NOAA-ESRL. We thank D. Longenecker and T. Mefford of NOAA-ESRL for their processing and dissemination of the BRW data. Recognition is also extended to those responsible for the operation and maintenance of the instruments that produced the data used in this study; their diligent and dedicated efforts are often underappreciated.

References

- Ackerman, T. P., and G. M. Stokes (2003), The Atmospheric Radiation Measurement Program, *Phys. Today*, *56*(1), 38–44.
- Clothiaux, E. E., T. P. Ackerman, G. G. Mace, K. P. Moran, R. T. Marchand, M. A. Miller, and B. E. Martner (2000), Objective determination of cloud heights and radar reflectivities using a Combination of active remote sensors at the Atmospheric Radiation Measurement Program Cloud and Radiation Test Bed (ARM CART) sites, *J. Appl. Meteorol.*, *39*, 645–665.
- Comiso, J. C., C. L. Parkinson, R. Gersten, and L. Stock (2008), Accelerated decline in the Arctic sea ice cover, *Geophys. Res. Lett.*, *35*, L01703, doi:10.1029/2007GL031972.
- Curry, J. A., W. B. Rossow, D. Randall, and J. L. Schramm (1996), Overview of Arctic cloud and radiation characteristics, *J. Clim.*, *9*, 1731–1764.
- Curry, J. A., and coauthors (2000), FIRE Arctic Clouds Experiment, *Bull. Am. Meteorol. Soc.*, *81*, 5–29.
- Dong, X., and G. G. Mace (2003), Arctic stratus cloud properties and radiative forcing derived from ground-based data collected at Barrow, Alaska, *J. Clim.*, *16*(3), 445–461.
- Dong, X., P. Minnis, T. P. Ackerman, E. E. Clothiaux, G. G. Mace, C. N. Long, and J. C. Liljegren (2000), A 25-month database of stratus cloud properties generated from ground-based measurements at the ARM SGP site, *J. Geophys. Res.*, *105*, 4529–4538, doi:10.1029/1999JD901159.
- Dong, X., P. Minnis, and B. Xi (2005), A climatology of midlatitude continental clouds from ARM SGP site. Part I: Low-level cloud macrophysical, microphysical and radiative properties, *J. Clim.*, *18*, 1391–1410.
- Dong, X., B. Xi, and P. Minnis (2006a), A climatology of midlatitude continental clouds from the ARM SGP Central Facility: Part II: Cloud fraction and surface radiative forcing, *J. Clim.*, *19*, 1765–1783.
- Dong, X., B. Xi, and P. Minnis (2006b), Observational evidence of changes in water vapor, clouds, and radiation at the ARM SGP site, *Geophys. Res. Lett.*, *33*, L19818, doi:10.1029/2006GL027132.
- Durr, B., and R. Philipona (2004), Automatic cloud amount detection by surface longwave downward radiation measurements, *J. Geophys. Res.*, *109*, D05201, doi:10.1029/2003JD004182.

- Feng, Z., X. Dong, and B. Xi (2009), A study of the vertical profile and evaluation of convective systems using a merged MMCR and WSR-88D database at the SGP site, *J. Atmos. Oceanic Technol.*, *26*, 958–971.
- Gates, W. L. (1992), AMIP: The atmospheric model intercomparison project, *Bull. Am. Meteorol. Soc.*, *73*, 1962–1970.
- GMCC; Geophysical Monitoring for Climatic Change (1974), No. 1, Summary Report 1972, edited by J. M. Miller, U.S. Dept. of Commerce, NOAA Environ. Res. Lab., Boulder, Colo.
- Intrieri, J. M., M. D. Shupe, T. Uttal, and B. J. McCarty (2002a), An annual cycle of Arctic cloud characteristics observed by radar and lidar at SHEBA, *J. Geophys. Res.*, *107*(C10), 8030, doi:10.1029/2000JC000423.
- Intrieri, J. M., C. W. Fairall, M. D. Shupe, P. O. G. Persson, E. L. Andreas, P. S. Guest, and R. E. Moritz (2002b), An annual cycle of Arctic surface cloud forcing at SHEBA, *J. Geophys. Res.*, *107*(C10), 8039, doi:10.1029/2000JC000439.
- Kato, S., T. P. Ackerman, E. E. Clothiaux, J. H. Mather, G. G. Mace, M. L. Wesely, F. Murray, and J. Michalsky (1997), Uncertainties in modeled and measured clear-sky surface shortwave irradiances, *J. Geophys. Res.*, *102*, 25,881–25,898, doi:10.1029/97JD01841.
- Kay, J. E., T. L'Ecuyer, A. Gettelman, G. Stephens, and C. O'Dell (2008), The contribution of cloud and radiation anomalies to the 2007 Arctic sea ice extent minimum, *Geophys. Res. Lett.*, *35*, L08503, doi:10.1029/2008GL033451.
- Kennedy, J. J., H. A. Titchner, J. Hardwick, M. Beswick, and D. E. Parker (2007), Global and regional climate in 2007, *Weather*, *62*, 232–242.
- Kennedy, A., X. Dong, B. Xi, P. Minnis, A. Del Genio, A. Wolf, and M. Khaiver (2010), Evaluation of the NASA GISS Single Column Model simulated clouds using combined surface and satellite observations, *J. Clim.*, doi:10.1175/2010JCLI3353.1.
- Liljegren, J. C., E. E. Clothiaux, G. G. Mace, S. Kato, and X. Dong (2001), A new retrieval for cloud liquid water path using a ground-based microwave radiometer and measurements of cloud temperature, *J. Geophys. Res.*, *106*, 14,485–14,500, doi:10.1029/2000JD900817.
- Long, C. N. (2004), The next-generation flux analysis: Adding clear-sky LW and LW cloud effects, cloud optical depths, and improved sky cover estimates, paper presented at Fourteenth Atmospheric Radiation Measurement (ARM) Science Team Meeting, Albuquerque, N. M., 22–26 March.
- Long, C. N. (2005), On the estimation of clear-sky upwelling SW and LW, 15th ARM Science Team Meeting Proceedings, Daytona Beach, Fla, 14–18 March.
- Long, C. N., and D. D. Turner (2008), A method for continuous estimation of clear-sky downwelling longwave radiative flux developed using ARM surface measurements, *J. Geophys. Res.*, *113*, D18206, doi:10.1029/2008JD009936.
- Long, C. N., and T. P. Ackerman (2000), Identification of clear skies from broadband pyranometer measurements and calculation of downwelling shortwave cloud effects, *J. Geophys. Res.*, *105*, 15,609–15,626, doi:10.1029/2000JD900077.
- Long, C. N., and Y. Shi (2008), An automated quality assessment and control algorithm for surface radiation measurements, *J. Open Atmos. Sci.*, *2*, 23–37.
- Mace, G. G., and coauthors (2006), Cloud radiative forcing at the Atmospheric Radiation Measurement Program Climate Research Facility: 1. Technique, validation, and comparison to satellite-derived diagnostic quantities, *J. Geophys. Res.*, *111*, D11S90, doi:10.1029/2005JD005921.
- Marty, C., and R. Philipona (2000), The clear-sky index to separate clear-sky situations in climate research, *Geophys. Res. Lett.*, *27*, 1641–1644, doi:10.1029/2000GL011743.
- Marty, C., R. Philipona, J. Delamere, E. G. Dutton, J. Michalsky, K. Stamnes, R. Storvold, T. Stoffel, S. A. Clough, and E. J. Mlawer (2003), Downward longwave irradiance uncertainty under arctic atmospheres: Measurements and modeling, *J. Geophys. Res.*, *108*(D12), 4358, doi:10.1029/2002JD002937.
- Maykut, G. A., and N. Untersteiner (1971), Some results from a time-dependent thermodynamic model of sea ice, *J. Geophys. Res.*, *76*, 1550–1575, doi:10.1029/JC076i006p01550.
- Mitchell, J. F. B., and W. J. Ingram (1992), Carbon dioxide and climate: Mechanisms of changes in cloud, *J. Clim.*, *5*, 5–21.
- Moran, K. P., B. E. Martner, M. J. Post, R. A. Kropfli, D. C. Welsh, and K. B. Widener (1998), An unattended cloud-profiling radar for use in climate research, *Bull. Am. Meteorol. Soc.*, *79*, 443–455.
- Perovich, D. K., and coauthors (1999), Year on ice gives climate insights, *Eos Trans. AGU*, *80*, 481.
- Randall, D., and coauthors (1998), Status of and outlook for large-scale modeling of atmospheric-ice-ocean interactions in the Arctic, *Bull. Am. Meteorol. Soc.*, *78*, 197–219.
- Ramanathan, V., R. D. Cess, E. F. Harrison, P. Minnis, B. R. Barkstrom, E. Ahmad, and D. Hartmann (1989), Cloud-radiative forcing and climate: Results from the Earth Radiation Budget Experiment, *Science*, *243*, 57–63.
- Richter-Menge, J., et al. (2008), Arctic Report Card 2008. <http://www.noaa/arctic/gov/reportcard/>.
- Schweiger, A. J., J. Zhang, R. W. Lindsay, and M. Steele (2008), Did unusually sunny skies help drive the record sea ice minimum, *Geophys. Res. Lett.*, *35*, L10503, doi:10.1029/2008GL033463.
- Shupe, M., and J. M. Intrieri (2004), Cloud radiative forcing of the arctic surface: The influence of cloud properties, surface albedo, and solar zenith angle, *J. Clim.*, *17*, 616–628.
- Shulski, M., and G. Wendler (2007), *The Climate of Alaska*, Univ. of Alaska Press, Fairbanks.
- Stamnes, K., R. G. Ellingson, J. A. Curry, J. E. Walsh, and B. D. Zak (1999), Review of science issues, development strategy, and status for the ARM North Slope of Alaska-Adjacent Arctic Ocean climate research site, *J. Clim.*, *12*, 46–63.
- Stone, R. S. (1997), Variations in western Arctic temperatures in response to cloud radiative and synoptic-scale influences, *J. Geophys. Res.*, *102*, 21,769–21,776, doi:10.1029/97JD01840.
- Stone, R. S., E. G. Dutton, J. M. Harris, and D. Longenecker (2002), Earlier spring snowmelt in northern Alaska as an indicator of climate change, *J. Geophys. Res.*, *107*(D10), 4089, doi:10.1029/2000JD000286.
- Stone, R., T. Mefford, E. Dutton, D. Longenecker, B. Halter, and D. Endres (1996), Barrow, Alaska, surface radiation and meteorological measurements: January 1992 to December 1994, *NOAA Data Rep. ERL CMDL-11*, 81 pp., NOAA Clim. Monit. and Diagnostics Lab., Boulder, Colo.
- Stroeve, J., M. Serezee, S. Drobot, S. Gearheard, M. Holland, J. Maslanik, W. Meier, and T. Scambos (2008), Arctic sea ice extent plummets in 2007, *Eos Trans. AGU*, *29*, 13.
- Tao, X., J. E. Walsh, and W. L. Chapman (1996), An assessment of global climate simulations of Arctic air temperatures, *J. Clim.*, *9*, 1060–1076.
- Uttal, T., and coauthors (2002), Surface heat budget of the Arctic Ocean, *Bull. Am. Meteorol. Soc.*, *83*, 255–275.
- Verlinde, J., and coauthors (2007), The Mixed-Phase Arctic Cloud Experiment, *Bull. Am. Meteorol. Soc.*, *88*, 205–221.
- Wang, Z., and K. Sassen (2002), Cirrus cloud microphysical properties retrieval using lidar and radar measurements. Part II: Midlatitude cirrus microphysical and radiative properties, *J. Atmos. Sci.*, *59*(14), 2291–2302.
- Wang, X., and J. R. Key (2005), Arctic surface, cloud, and radiation properties based on the AVHRR polar Pathfinder data set. Part I: Spatial and temporal characteristics, *J. Clim.*, *18*, 2558–2574.
- Wetherald, R. T., and S. Manabe (1988), Cloud feedback processes in general circulation model, *J. Atmos. Sci.*, *45*, 1397–1415.
- Xi, B., X. Dong, P. Minnis, and M. M. Khaiyer (2010), A 10 year climatology of cloud fraction and vertical distribution derived from both surface and GOES observations over the DOE ARM SPG site, *J. Geophys. Res.*, *115*, D12124, doi:10.1029/2009JD012800.
- Younkin, K., and C. N. Long (2003), Improved correction of IR loss in diffuse shortwave measurements: AM ARM value-added product, *DOE ARM Tech. Rep. TR-09*, Richland, Wash. (Available at http://www.arm.gov/publications/tech_reports/arm-tr-009.pdf).

K. Crosby, X. Dong, and B. Xi, Department of Atmospheric Sciences, University of North Dakota, 4149 University Ave., Stop 9006, Grand Forks, ND 58202-9006, USA. (dong@aero.und.edu)

C. N. Long, Pacific Northwest National Laboratory, U.S. Department of Energy, Richland, WA 99352, USA.

M. D. Shupe and R. S. Stone, Cooperative Institute for Research in Environmental Sciences, University of Colorado at Boulder, Boulder, CO 80309, USA.